Quantum simulation experiments with superconducting circuits

Zur Erlangung des akademischen Grades eines
Doktors der Naturwissenschaften
der Fakultät für Physik des
Karlsruher Instituts für Technologie (KIT)

genehmigte
Dissertation
von

M. Sc. Jochen Braumüller

Contents

1 Introduction

Understanding basic principles and phenomena in nature has been a perpetual motivation for researchers since the beginning of mankind. Classical computers, acting as universal computational devices in the sense of deterministic Turing machines [Tur37], provide a powerful tool to efficiently simulate the dynamics of physical systems obeying Newtonian physics. With the advent of quantum mechanics, it became however apparent that the properties and dynamics of microscopic systems in particular are not captured by classical physics in general. A quantum mechanical treatment is typically required on atomic scales, for instance in order to treat single molecules or proteins of biological systems or general quantum models in condensed matter physics. These quantum problems have been proven incompatible with the original Turing hypothesis [Deu85] and resilient to be efficiently simulated with classical computers. However, it was proposed [Fey82; Deu85] and verified [Llo96] that any physical system can be simulated by a universal quantum computer.
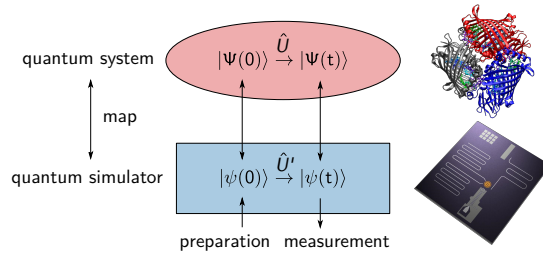
Figure 1.1: Analog quantum simulation A quantum system of interest (red), artistically depicted as a protein complex, is mapped onto an artificial quantum simulator (blue). In this thesis the quantum simulator is a superconducting circuit. By preparing and reading out quantum states $|\psi\rangle$ of the simulator system, the time evolution $\hat{U}$ of the underlying quantum problem, described by the state $|\Psi\rangle$, can be inferred [GAN14].

The quest in quantum simulation, which comes in two flavours, is to solve the time evolution of a certain quantum system of interest.

The framework of analog quantum simulation, used in this thesis, is schematically depicted in Fig. 1.1. A quantum system of interest is mapped onto a tailored and well controllable artificial quantum system, striving to mimic the dynamics of

the investigated quantum system. In the setting of this thesis, the simulator is a superconducting quantum circuit. When approximately the same equations of motion hold for both systems, the solution of the underlying quantum problem can be inferred from observing the time evolution of the artificially built model system.

2 Microwave theory

This chapter provides the fundamentals of microwave theory necessary for evaluating and characterising quantum circuits. I give a brief summary of transmission line theory and its circuit implementation which is followed by some network analysis techniques. The description of microwave resonators is carried out in more detail. Despite of its importance for a large community of microwave engineers as well as to the field of circuit based quantum information processing, I find a lack of a comprehensive treatment of respective fitting models in literature. To this end, I derive relevant formulas relating the experimentally accessible scattering matrix elements with the frequency response of microwave resonators, providing the mathematical framework for extracting quality factors of resonating networks based on circuit impedances.

Given that the magnitude signal $|S^{\text{s}}_{11}|^2$ is very small for strongly over-coupled resonators, a robust method to extract resonator characteristics is provided by fitting the frequency derivative of the phase to a Lorentzian distribution. In Fig. (**??**)(c), (d) we compare Lorentzian fits to the derivative of the phase quadrature $\partial/\partial\omega \arg S^{\text{s}}_{11}$ and to the inverted and shifted phase quadrature, $\partial/\partial\omega \arg(1 - S^{\text{s}}_{11})$. While the latter is the analytically exact procedure, it requires an elaborate post-processing of measured data, such as a normalization and a slope subtraction in the phase signal, which is physically hard to justify. Comparing the extracted loaded quality factors demonstrates the reliability of the straightforward method. The internal quality factor in the example is $\sim 20 \times 10^3$.

Table 2.1: Summary of relations between scattering matrix elements and frequency response of relevant one- and two-port resonator networks In the in-line configuration, a resonator is defined by introducing two gaps in a continuous transmission line. The reflection case is analog to single-port reflection, with individual coupling quality factors $Q_{c,i}$ for port $i = 1, 2$, respectively. For equal coupling capacitors at either port, we can recover $S_{11}^{il,i} = S_{11}^{s}$ for $Q_c = Q_{c,i}/2$. The in-line transmission matrix element S_{21}^{il} is provided with respect to a the total coupling quality factor $Q_{c,\Sigma}^{-1} = Q_{c,1}^{-1} + Q_{c,2}^{-1}$.

	scattering matrix elem.	magnitude squared	phase
notch	$S_{21}^{n} = 1 - \dfrac{Q_L/Q_c}{1+2iQ_L\frac{\Delta\omega}{\omega_0}}$	$\lvert S_{21}^{n}\rvert^2 = 1 - \dfrac{1-(Q_L-Q_c)^2/Q_c^2}{1+4Q_L^2\left(\frac{\Delta\omega}{\omega_0}\right)^2}$	$\arg S_{21}^{n} = -\arctan\left(2Q_L\frac{\Delta\omega}{\omega_0}\right) - \arctan\left(2\frac{Q_LQ_c}{Q_L-Q_c}\frac{\Delta\omega}{\omega_0}\right)$
	$S_{11}^{n} = \dfrac{Q_L/Q_c}{1+2iQ_L\frac{\Delta\omega}{\omega_0}}$	$\lvert S_{11}^{n}\rvert^2 = \dfrac{(Q_L/Q_c)^2}{1+4Q_L^2\left(\frac{\Delta\omega}{\omega_0}\right)^2}$	$\arg S_{11}^{n} = -\arctan\left(2Q_L\frac{\Delta\omega}{\omega_0}\right)$
single port	$S_{11}^{s} = 1 - \dfrac{2Q_L/Q_c}{1+2iQ_L\frac{\Delta\omega}{\omega_0}}$	$\lvert S_{11}^{s}\rvert^2 = 1 - \dfrac{1-(2Q_L-Q_c)^2/Q_c^2}{1+4Q_L^2\left(\frac{\Delta\omega}{\omega_0}\right)^2}$	$\arg S_{11}^{s} = -\arctan\left(2Q_L\frac{\Delta\omega}{\omega_0}\right) - \arctan\left(2\frac{Q_LQ_c}{2Q_L-Q_c}\frac{\Delta\omega}{\omega_0}\right)$
in-line	$S_{21}^{il} = \dfrac{Q_L/Q_{c,\Sigma}}{1+2iQ_L\frac{\Delta\omega}{\omega_0}}$	$\lvert S_{21}^{il}\rvert^2 = \dfrac{(Q_L/Q_{c,\Sigma})^2}{1+4Q_L^2\left(\frac{\Delta\omega}{\omega_0}\right)^2}$	$\arg S_{21}^{il} = -\arctan\left(2Q_L\frac{\Delta\omega}{\omega_0}\right)$
	$S_{11}^{il,i} = 1 - \dfrac{2Q_L/Q_{c,i}}{1+2iQ_L\frac{\Delta\omega}{\omega_0}}$	$\lvert S_{11}^{il,i}\rvert^2 = 1 - \dfrac{1-(2Q_L-Q_{c,i})^2/Q_{c,i}^2}{1+4Q_L^2\left(\frac{\Delta\omega}{\omega_0}\right)^2}$	$\arg S_{11}^{il,i} = -\arctan\left(2Q_L\frac{\Delta\omega}{\omega_0}\right) - \arctan\left(2\frac{Q_LQ_{c,i}}{2Q_L-Q_{c,i}}\frac{\Delta\omega}{\omega_0}\right)$

3 The concentric transmon qubit

Some words with a Ref. [Bra+16].

3.1 Motivation

Over the last decade there has been a two order of magnitude increase in coherence times of superconducting qubits, which allowed for several major achievements in the pursuit of scalable quantum computation, such as the control and entanglement of multiple qubits [Ste+06; Bar+14]. Further increases in coherence times will eventually allow for building a fault tolerant quantum computer with a reasonable overhead in terms of error correction, as well as implementing novel quantum simulation schemes by accessing wider experimental parameter ranges [Par14]. Apart from the demand for advancing qubit lifetimes and coherence times, other properties become more and more important, such as the scalability of quantum circuits and the coupling versatility between qubits.

The design and architecture of the concentric transmon qubit is depicted in Fig. 3.1(a).

3.2 Dissipative dynamics

The dissipative dynamics of the investigated concentric transmon is depicted in Fig. **??**. At a qubit operation frequency of $\epsilon/2\pi = 6.85\,\text{GHz}$ we extract $T_1 = 9.6\,\mu\text{s}$ by exciting the qubit with a previously calibrated π pulse and measuring its population after varying times Δt. We engineered the concentric transmon to have a reduced sensitivity to its major loss channels, namely spontaneous Purcell emission, dielectric loss, and radiative decay. Losses due to quasi-particle tunneling processes typically impose a T_1 limitation at around $\sim 1\,\text{ms}$ [Ris+13], having no considerable effect on the lifetime of our circuit.

In the following, we provide a loss participation ratio analysis in order to explain the measured value for T_1. The results are summarized in Tab. 3.1.
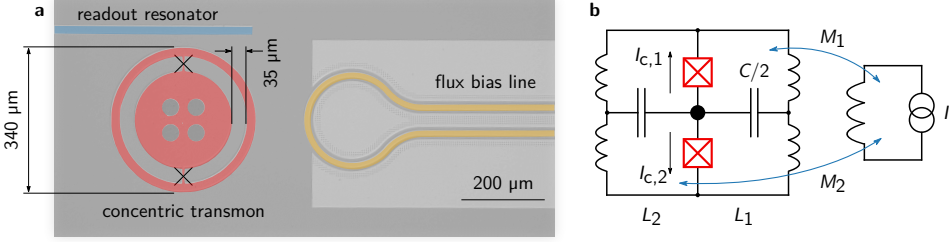
Figure 3.1: Architecture of the concentric transmon qubit (a) Optical micrograph of the fabricated sample. The dark grey colour corresponds to the intrinsic silicon substrate, while the coloured and brighter areas are covered with an Al film. The transmon consists of a central island with holes for flux trapping, that is surrounded by a concentric ring electrode. The electrodes are interconnected by two Josephson junctions, forming a gradiometric dc SQUID. The open end of a microstrip $\lambda/2$-resonator (coloured in blue) capacitively couples to the concentric transmon for dispersive qubit readout. An on-chip flux bias coil (yellow) allows for fast tuning of the qubit transition frequency since it couples asymmetrically to the two SQUID loops. It is designed in coplanar geometry in order to match its impedance to $50\,\Omega$. The flux bias line is grounded at one of its ends on chip. A superconducting groundplane is applied to the backside of the substrate. (b) Simplified lumped-element circuit diagram. The black dot in the middle corresponds to the central qubit island. One can recognize two closed loops (L_1, L_2) sharing the two Josephson junctions. The large loop size in the geometry amounts to a geometric inductance contribution, as indicated in the circuit. Since the mutual inductances to the flux bias line are not equal, $M_1 \neq M_2$, the effective critical current of the SQUID can be tuned.

Table 3.1: Calculated loss contributions fo the concentric transmon qubit The main contribution $\Gamma_{1,\text{ind}}^{-1}$ arises from inductive coupling to the flux bias line, leading to a total Purcell limitation of $\Gamma_{1,P}^{-1} = 16\,\mu\text{s}$. The estimated reciprocal sum Γ_Σ^{-1} is in good agreement with the measured value for T_1.

Purcell			Defects	Radiation	Reciprocal sum
$\Gamma_{1,\text{sm}}^{-1}$	$\Gamma_{1,\text{ind}}^{-1}$	$\Gamma_{1,\text{cap}}^{-1}$	$\Gamma_{1,\text{TLF}}^{-1}$	$\Gamma_{1,\text{rad}}^{-1}$	Γ_Σ^{-1}
$47\,\mu\text{s}$	$32\,\mu\text{s}$	$\sim 87\,\mu\text{s}$			
	$\Gamma_{1,P}^{-1} = 16\,\mu\text{s}$		$\sim 26\,\mu\text{s}$	$\gtrsim 100\,\mu\text{s}$	$8.9\,\mu\text{s}$

3.2.1 Purcell decay

We find a coupling limited decay rate $\kappa = 26 \times 10^6\,\text{s}^{-1}$, corresponding to a line width of $4.1\,\text{MHz}$ of the dispersive readout resonator, which is close to the design value. The qubit lifetime is potentially Purcell limited by spontaneous emission into modes that are nearby in frequency. Major contributions are the dispersive single-mode decay into the capacitively coupled readout resonator as well as emission into the flux bias line [Koc+07; Hou+08] due to inductive coupling. The coupling strength

$g/2\pi = 55\,\text{MHz}$ between qubit and resonator is extracted from the dispersive shift of the resonator [Bra+15].

3.3 Conclusion

We have designed, fabricated and experimentally investigated a planar tunable qubit based on superconducting circuits that we call concentric transmon.

4 Conclusion

It is my conviction that the universal quantum computer will be a truly digital device while meaningful computations with quantum hardware in the near future will be based on analog simulation schemes. This thesis presents a small contribution in this direction.

Bibliography

[Bar+14]   R. Barends, J. Kelly, A. Megrant, A. Veitia, D. Sank, E. Jeffrey, T. C. White, J. Mutus, A. G. Fowler, B. Campbell, Y. Chen, B. Chiaro, A. Dunsworth, C. Neill, P. O'Malley, P. Roushan, A. Vainsencher, J. Wenner, A. N. Korotkov, A. N. Cleland, and J. M. Martinis: *Superconducting quantum circuits at the surface code threshold for fault tolerance*. Nature **508**.7497 (2014), pp. 500–503. DOI: `10.1038/nature13171` (cit. on p. 5).

[Bra+15]   J. Braumüller, J. Cramer, S. Schlör, H. Rotzinger, L. Radtke, A. Lukashenko, P. Yang, S. T. Skacel, S. Probst, M. Marthaler, L. Guo, A. V. Ustinov, and M. Weides: *Multiphoton dressing of an anharmonic superconducting many-level quantum circuit*. Phys. Rev. B **91**.5 (2015), p. 054523. DOI: `10.1103/physrevb.91.054523` (cit. on p. 7).

[Bra+16]   J. Braumüller, M. Sandberg, M. R. Vissers, A. Schneider, S. Schlör, L. Grünhaupt, H. Rotzinger, M. Marthaler, A. Lukashenko, A. Dieter, A. V. Ustinov, M. Weides, and D. P. Pappas: *Concentric transmon qubit featuring fast tunability and an anisotropic magnetic dipole moment*. Appl. Phys. Lett. **108**.3 (2016), p. 032601. DOI: `10.1063/1.4940230` (cit. on p. 5).

[Deu85]   D. Deutsch: *Quantum Theory, the Church-Turing Principle and the Universal Quantum Computer*. Proc. R. Soc. Lond. A. Vol. 400. 1818. The Royal Society, 1985, pp. 97–117. DOI: `10.1098/rspa.1985.0070` (cit. on p. 1).

[Fey82]   R. P. Feynman: *Simulating physics with computers*. Int. J. Theor. Phys. **21**.6-7 (1982), pp. 467–488. DOI: `10.1007/BF02650179` (cit. on p. 1).

[GAN14]   I. M. Georgescu, S. Ashhab, and F. Nori: *Quantum simulation*. Rev. Mod. Phys. **86**.1 (2014), pp. 153–185. DOI: `10.1103/revmodphys.86.153` (cit. on p. 1).

[Hou+08]   A. A. Houck, J. A. Schreier, B. R. Johnson, J. M. Chow, J. Koch, J. M. Gambetta, D. I. Schuster, L. Frunzio, M. H. Devoret, S. M. Girvin, and R. J. Schoelkopf: *Controlling the Spontaneous Emission of a Superconducting Transmon Qubit*. Phys. Rev. Lett. **101**.8 (2008), p. 080502. DOI: `10.1103/physrevlett.101.080502` (cit. on p. 6).

[Koc+07]   J. Koch, T. M. Yu, J. Gambetta, A. A. Houck, D. I. Schuster, J. Majer, A. Blais, M. H. Devoret, S. M. Girvin, and R. J. Schoelkopf: *Charge-insensitive qubit design derived from the Cooper pair box*. Phys. Rev. A **76** (2007), p. 042319. DOI: `10.1103/PhysRevA.76.042319` (cit. on p. 6).

[Llo96]   S. Lloyd: *Universal Quantum Simulators*. Science **273** (1996), pp. 1073–1078. DOI: `10.1126/science.273.5278.1073` (cit. on p. 1).

[Pai+11]   H. Paik, D. I. Schuster, L. S. Bishop, G. Kirchmair, G. Catelani, A. P. Sears, B. R. Johnson, M. J. Reagor, L. Frunzio, L. I. Glazman, S. M. Girvin, M. H. Devoret, and R. J. Schoelkopf: *Observation of High Coherence in Josephson Junction Qubits Measured in a Three-Dimensional Circuit QED Architecture*. Phys. Rev. Lett. **107**.24 (2011). DOI: `10.1103/PhysRevLett.107.240501`.

[Par14]   G. S. Paraoanu: *Recent Progress in Quantum Simulation Using Superconducting Circuits*. J. Low Temp. Phys. **175**.5-6 (2014), pp. 633–654. DOI: `10.1007/s10909-014-1175-8` (cit. on p. 5).

[Pop+14]   I. M. Pop, K. Geerlings, G. Catelani, R. J. Schoelkopf, L. I. Glazman, and M. H. Devoret: *Coherent suppression of electromagnetic dissipation due to superconducting quasiparticles*. Nature **508** (2014), pp. 369–372. DOI: `10.1038/nature13017`.

[Rig+12]   C. Rigetti, J. M. Gambetta, S. Poletto, B. L. T. Plourde, J. M. Chow, A. D. Córcoles, J. A. Smolin, S. T. Merkel, J. R. Rozen, G. A. K. Keefe, M. B. Rothwell, M. B. Ketchen, and S. M.: *Superconducting qubit in a waveguide cavity with a coherence time approaching 0.1 ms*. Phys. Rev. B **86**.10 (2012), p. 100506. DOI: `10.1103/physrevb.86.100506`.

[Ris+13]   D. Ristè, C. C. Bultink, M. J. Tiggelman, R. N. Schouten, K. W. Lehnert, and L. DiCarlo: *Millisecond charge-parity fluctuations and induced decoherence in a superconducting transmon qubit*. Nat. Commun. **4** (2013), p. 1913. DOI: `10.1038/ncomms2936` (cit. on p. 5).

[San+13]   M. Sandberg, M. R. Vissers, T. A. Ohki, J. Gao, J. Aumentado, M. Weides, and D. P. Pappas: *Radiation-suppressed superconducting quantum bit in a planar geometry*. Appl. Phys. Lett. **102**.7 (2013), p. 072601. DOI: `10.1063/1.4792698`.

[Ste+06]   M. Steffen, M. Ansmann, R. C., N. Bialczak, E. L. Katz, R. McDermott, M. Neeley, E. M. Weig, A. N. Cleland, and J. M. Martinis: *Measurement of the Entanglement of Two Superconducting Qubits via State Tomography*. Science **313**.5792 (2006), pp. 1423–1425. DOI: `10.1126/science.1130886` (cit. on p. 5).

[Tur37]   A. M. Turing: *On Computable Numbers, with an Application to the Entschei-dungsproblem. Proc. Lond. math. Soc. Ser. 2*. Vol. s2-42. 1. 1937, pp. 230–265. DOI: `10.1112/plms/s2-42.1.230` (cit. on p. 1).

List of publications

[Bra+15]   J. Braumüller, J. Cramer, S. Schlör, H. Rotzinger, L. Radtke, A. Lukas-henko, P. Yang, S. T. Skacel, S. Probst, M. Marthaler, L. Guo, A. V. Ustinov, and M. Weides: *Multiphoton dressing of an anharmonic superconducting many-level quantum circuit*. Phys. Rev. B **91**.5 (2015), p. 054523. DOI: `10.1103/physrevb.91.054523`.

[Bra+17]   J. Braumüller, M. Marthaler, A. Schneider, A. Stehli, H. Rotzinger, M. Weides, and A. V. Ustinov: *Analog quantum simulation of the Rabi model in the ultra-strong coupling regime*. Nat. Commun. **8**.1 (2017), p. 779. DOI: `10.1038/s41467-017-00894-w`.

[Bra+16]   J. Braumüller, M. Sandberg, M. R. Vissers, A. Schneider, S. Schlör, L. Grünhaupt, H. Rotzinger, M. Marthaler, A. Lukashenko, A. Dieter, A. V. Ustinov, M. Weides, and D. P. Pappas: *Concentric transmon qubit featuring fast tunability and an anisotropic magnetic dipole moment*. Appl. Phys. Lett. **108**.3 (2016), p. 032601. DOI: `10.1063/1.4940230`.

[Lep+17]   J. Leppäkangas, J. Braumüller, A. V. Ustinov, M. Weides, and M. Marthaler: *Quantum simulation of the spin-boson model in a microwave circuit*. Preprint at `https://arxiv.org/abs/1711.07463`. (2017).

[Rei+16]   J.-M. Reiner, M. Marthaler, J. Braumüller, M. Weides, and G. Schön: *Emulating the one-dimensional Fermi-Hubbard model by a double chain of qubits*. Phys. Rev. A **94**.3 (2016), p. 032338. DOI: `10.1103/physreva.94.032338`.

Appendix

A   Fabrication parameters

Table 1: Substrate cleaning

solvent	ultrasonic bath	IPA	H$_2$O	hot plate	piranha rinse
NEP	10 min	yes	yes	145 °C, 1 min	yes

A.1   Electron beam lithography

Table 2: Application of the resist stack

resist	pre	spin	hotplate
LOR 500nm	300 rpm, 10 s	3000 rpm, 60 s	180 °C, 5 min
PMMA 950K AR-P672.03	300 rpm, 10 s	6000 rpm, 60 s	145 °C, 5 min

Acknowledgements

Danke, Mama.